1-1-2007

Influence of dog-bone apex on shape during slab horizontal rolling process

Hai-liang Yu
Northeastern University, hailiang@uow.edu.au

Xiang-hua Liu
Northeastern University, liuxh@uow.edu.au

Chang-sheng Li
Northeastern University

Guo-dong Wang
Northeastern University

Influence of dog-bone apex on shape during slab horizontal rolling process

Abstract

The deformation of slab with dog-bone shape during the horizontal rolling process was simulated using FEM, and the influences of apical dislocation of dog-bone on the slab spread as well as the minimum crop end loss and the lost width at slab head and tail were analyzed. The results show that with the increase in the apical dislocation of dog-bone (LA), the slab spread and the minimum crop end loss at slab head and tail decrease, while the lost width at slab head and tail increases. Meanwhile, the relationships of S/LA-LA, LH/LA-LA, WH/LA-LA, LT/LA-LA, and WT/LA-LA were obtained. © 2007 Central Iron and Steel Research Institute.

Keywords

bone, influence, apex, dog, shape, during, slab, horizontal, rolling, process

Disciplines

Engineering | Science and Technology Studies

Publication Details

Yu, H., Liu, X., Li, C. & Wang, G. (2007). Influence of dog-bone apex on shape during slab horizontal rolling process. Journal of Iron and Steel Research International, 14 (3), 38-42.

Available online at www.sciencedirect.com

ScienceDirect

JOURNAL OF IRON AND STEEL RESEARCH, INTERNATIONAL. 2007, 14(3): 37-41

Influence of Dog-Bone Apex on Shape During Slab Horizontal Rolling Process

YU Hai-liang, LIU Xiang-hua, LI Chang-sheng, WANG Guo-dong

(State Key Laboratory of Rolling and Automation, Northeastern University, Shenyang 110004, Liaoning, China)

Abstract: The deformation of slab with dog-bone shape during the horizontal rolling process was simulated using FEM, and the influences of apical dislocation of dog-bone on the slab spread as well as the minimum crop end loss and the lost width at slab head and tail were analyzed. The results show that with the increase in the apical dislocation of dog-bone (L_A), the slab spread and the minimum crop end loss at slab head and tail decrease, while the lost width at slab head and tail increases. Meanwhile, the relationships of S/L_A-L_A, L_H/L_A-L_A, W_H/L_A-L_A, L_T/L_A-L_A, and W_T/L_A-L_A were obtained.

Key words: dog-bone; apical dislocation; horizontal rolling; FEM

The dog-bone shape is deformed in slabs during the vertical rolling process and the sizing press process and so on; this slab deformation and the action during the rolling process have been widely researched. For example, the rigid-plastic formulation and some simplified assumptions were taken into account by Mori K et al[1]; and the incremental viscoplastic model by David C et al[2] assumed a dog-bone shape as the function of friction; an non-steady state vertical-horizontal rolling process in roughing trains using the 3D finite element method (FEM) was studied by XIONG Shang-wu et al[3]; YU Hai-liang et al[4] researched the slab corner metal flow condition during the multi-pass V-H rolling process using FEM; LIU Hui et al[5] analyzed the effect of edger share on the slab profile with explicit dynamic FEM; and in the meantime, FENG Xian-zhang et al[6] employed the FEM to analyze the slab bulge distribution during sizing press (SP). The horizontal rolling for slabs with dog-bone shape was studied using 3D rigid-plastic FEM in Ref. [7], which proved that the FEM can be used to analyze the horizontal rolling process for slabs with dog-bone shape by comparing the calculated results and the experimental results. During the V-H rolling process and the SP process, the apical dislocation of dog-bone will change for different vertical roll shapes[4,5] and SP[6] rolling condition. However, no report on the influence of apical dislocation of 'dog-bone' on slab deformation has been found.

In this study, the horizontal rolling processes for slab with dog-bone shape were simulated under different apical dislocation of dog-bone using explicit dynamic FEM and the influences of the apical dislocation of dog-bone in slab on the slab deformation at head and tail, and spread were analyzed.

1 FEM Simulation

1.1 Basic parameters and rolling conditions

The horizontal rolling process for slab with dog-bone shape was simulated, and the diameter of the horizontal roll was 1 150 mm. The dimensions of the slab profile are shown in Fig. 1, in which the apical dislocation of dog-bone, L_A, is equal to 120 mm, 80 mm, 60 mm, 40 mm, 20 mm, 10 mm, 5 mm, respectively.

The main chemical composition of the slab is (mass percent, %): C 0.18, Si 0.32, and Mn 0.82. The

Foundation Item: Item Sponsored by State Basic Research Key Projects (973) of China (2006CB605208-1) and National Natural Science Foundation of China (50534020)

Biography: YU Hai-liang(1980-), Male, Doctor Candidate; **E-mail**: yuhailiang1980@tom.com; **Revised Date**: March 30, 2006

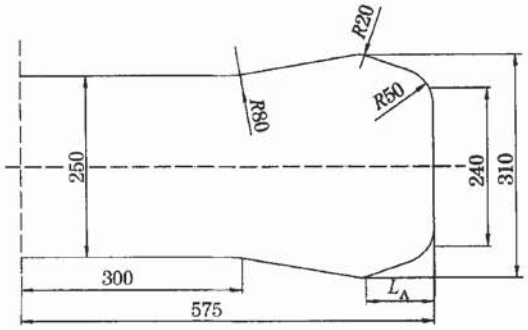

Fig. 1 Dimension of 'dog-bone' slab

yield stress at the high temperature is related to the true strain ε, the strain velocity $\dot{\varepsilon}$, and the deformation temperature T. During this simulation, the yield stresses were computed using Eqn. (1).

$$\sigma = A\varepsilon^{B}\dot{\varepsilon}^{CT+D}e^{FT} \quad (1)$$

where A, B, C, D, and F are constant.

During the rolling process, the rolling velocity is 4 m/s, and the slab draft is 10 mm; the coefficient of friction is 0.35.

1.2 Building of models

Owing to the symmetry of the slab with dog-bone shape and the rolls, 1/4 of the slab and rolls were included in the geometric model. The rolling models were built according to the parameters mentioned above. The rolls were considered as rigid body since their deformation could be neglected. At the same time, these just refined the element near the slab margin where the deformation assembled. The entire geometric model was dispersed with 8 nodes and hexahedral elements. The nodes on the bottom face of the slab were constrained in the Y direction, and the nodes on the center face of the slab were constrained in the X direction. The geometrical model and meshing of the rolling process are shown in Fig. 2. During simulation, the slab enters the roll with an initial velocity and aparts from the roll under the friction force. The time of entire rolling process is 0.5 s.

2 Results and Discussion

2.1 Slab spread

Table 1 shows the spread of slab at different L_A values. It can be seen that the spread of the slab decreases with the increase in L_A. When $L_A = 120$ mm, the spread of the slab is 19.1 mm, and when $L_A = 5$ mm, the spread of the slab is 25.9 mm.

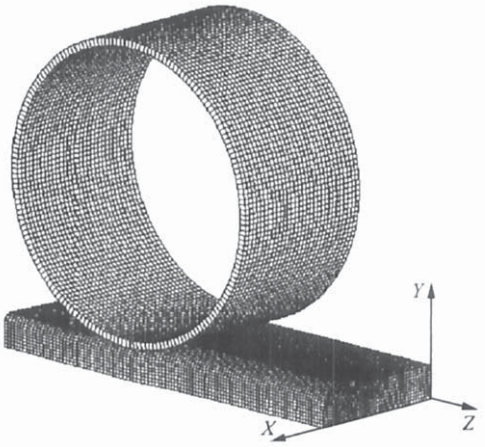

Fig. 2 FEM model for rolling process

Table 1 Slab spread

L_A/mm	120	80	60	40	20	10	5
Spread/mm	19.1	21.2	22.4	23.7	24.6	25.2	25.9

Fig. 3 shows the spread percentage of the slab at different L_A values. With the increase in L_A, the spread percentage decreases, and under the rolling condition, the spread percentage of the slab varies from 3.3% to 4.5%. By further analysis of the spread of the slab, let S/L_A [the ratio of spread of slab (S) to corresponding L_A] be Y axis and L_A be X axis, and the curve is drawn, as shown in Fig. 4. With the increase in L_A, S/L_A decreases. Thus, the curve can be fitted by Eqn. (2).

$$y = A_1 e^{(-x/t_1)} + A_2 e^{(-x/t_2)} + y_0 \quad (2)$$

where A_1, t_1, A_2, t_2, and y_0 are constants, and are set to be 11.741 51, 3.862 43, 2.201 11, 25.463 62, and 0.153 54, respectively, during the simulation.

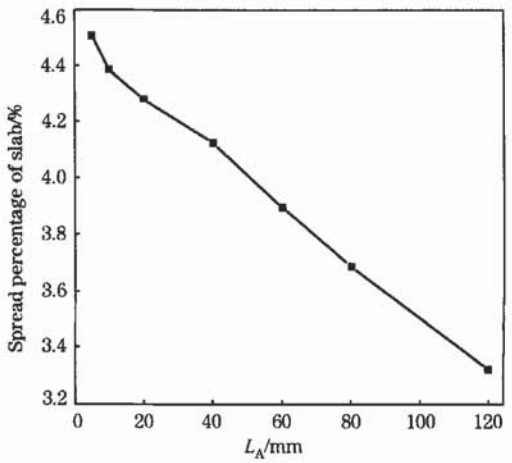

Fig. 3 Influence of apical dislocation of 'dog-bone' on spread percentage

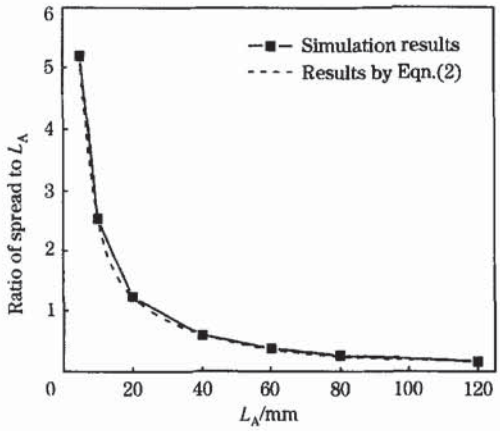

Fig. 4 Relationship between S/L_A and L_A

2.2 Deformation of slab head

Fig. 5 (a) shows the shape of the slab head after rolling at different L_A values, in which L_H is the minimum crop end loss at the slab head, and W_H is the lost width at slab head. Fig. 5 (b) shows the changing rules of L_H and W_H at different L_A values. It can be seen that W_H increases gradually with the increase in L_A, and the amplification is large, from 30 mm to 130 mm, whereas the L_H decreases gradually with the increase in L_A, from 45 mm to 36 mm.

Further analysis of L_H and W_H was carried out. Let L_A be the X axis, and L_H/L_A or W_H/L_A be the Y axis, the relationships of W_H/L_A-L_A, and L_H/L_A-L_A are shown in Fig. 6. It can be seen that the L_H/L_A and W_H/L_A decrease with the increase in L_A, and the relationships of W_H/L_A-L_A and L_H/L_A-L_A can be fitted by Eqn. (3) and Eqn. (4), respectively.

$$y=A_{13}e^{(-x/t_{13})}+A_{23}e^{(-x/t_{23})}+y_{03} \quad (3)$$

$$y=A_{14}e^{(-x/t_{14})}+A_{24}e^{(-x/t_{24})}+y_{04} \quad (4)$$

where A_{1i}, t_{1i}, A_{2i}, t_{2i}, y_{0i} are constants. During the simulation, the values of these constants are shown in Table 2.

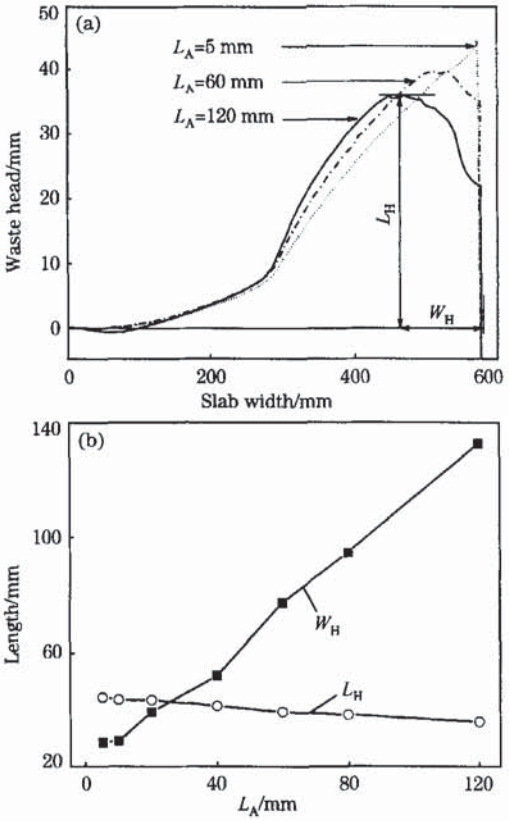

Fig. 5 Influence of L_A on deformation of slab head

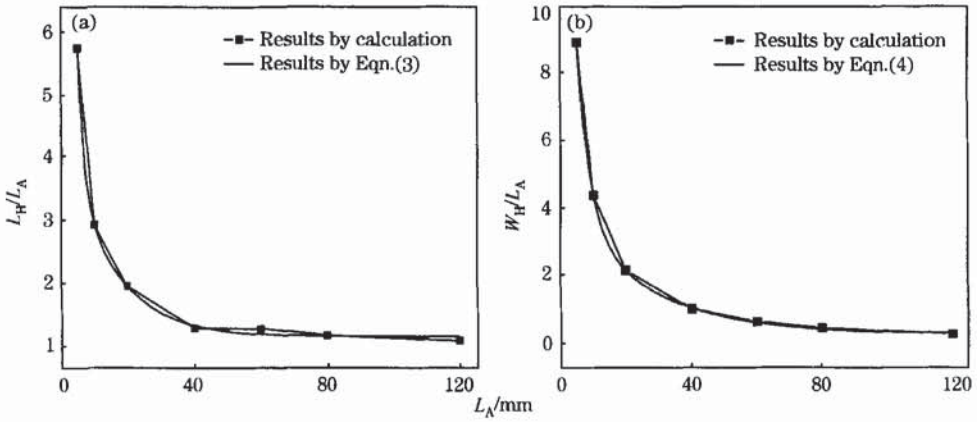

Fig. 6 Relationship of L_H/L_A and W_H/L_A to L_A

Table 2 Value of constant

Constant	A_{1i}	t_{1i}	A_{2i}	t_{2i}	y_{0i}
$i=3$	1.162 65	46.129 12	1.641 3	3.445 63	13.630 16
$i=4$	0.300 8	4.055 09	24.045 06	20.274 96	3.729 32

2.3 Deformation of slab tail

Fig. 7 (a) shows the shape of the slab tail after rolling at different L_A values, in which L_T is the minimum crop end loss at the slab tail, and W_T is the lost width at the slab tail. Fig. 7 (b) shows the changing rules of L_T and W_T at different L_A values. It can be seen that W_T increases gradually with the increase in L_A, from 35 mm to 140 mm, whereas the L_T decreases gradually with the increase in L_A, from 45 mm to 41 mm. By comparing Fig. 7 with Fig. 5, it can be found that the deformation level of the tail is larger than that of the head.

Further analysis of L_T and W_T was carried out. Let L_A be the X axis, and L_T/L_A or W_T/L_A be the Y axis, the relationships of L_T/L_A and W_T/L_A to L_A are shown in Fig. 8. It can be seen that the L_T/L_A and W_T/L_A values decrease with the increase in L_A, and the relationships of W_T/L_A and L_T/L_A to L_A can be fitted by Eqn. (5) and Eqn. (6), respectively.

$$y=A_{15}e^{(-x/t_{15})}+A_{25}e^{(-x/t_{25})}+y_{05} \quad (5)$$

$$y=A_{16}e^{(-x/t_{16})}+A_{26}e^{(-x/t_{26})}+y_{06} \quad (6)$$

where A_{1j}, t_{1j}, A_{2j}, t_{2j}, y_{0j} are constants. During the simulation, the values of these constants are shown in Table 3.

3 Conclusions

(1) The slab spread decreases as the apical dislocation of dog-bone L_A increases.

(2) The minimum crop end loss of slab head and tail decreases, and the lost width of slab head and tail increases as the apical dislocation of dog-bone L_A increases.

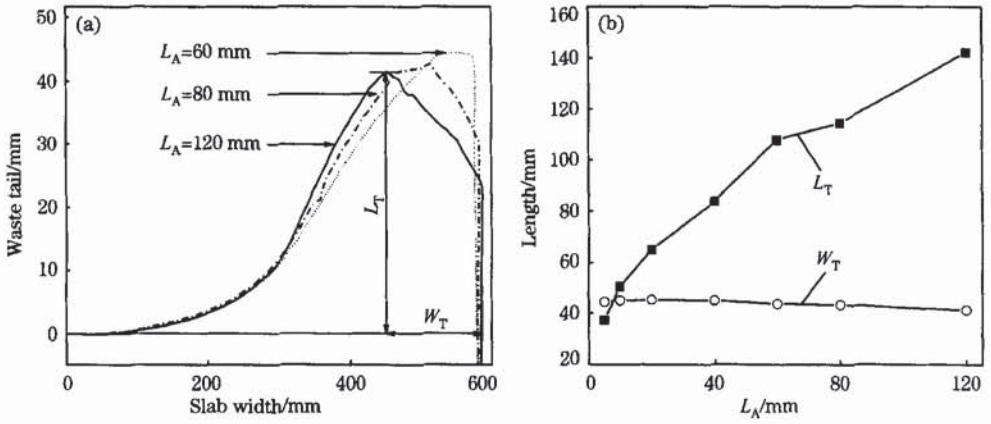

Fig. 7 Influence of L_A on deformation of slab tail

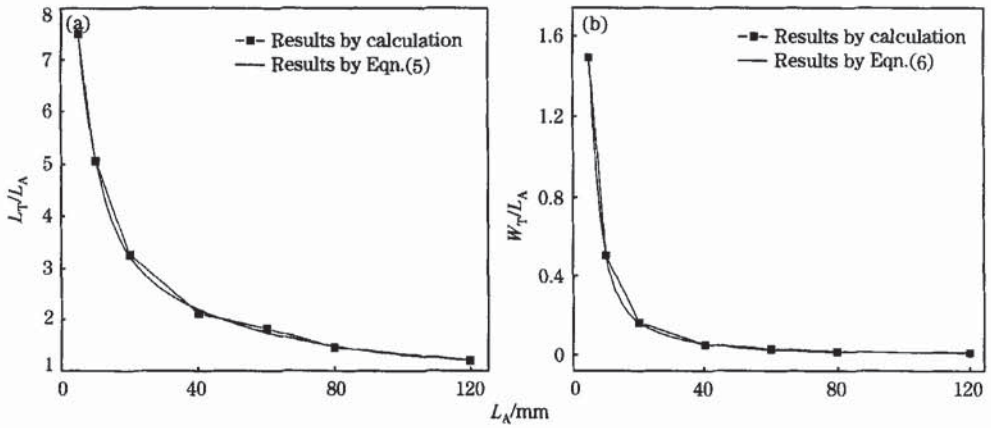

Fig. 8 Relationship of L_T/L_A and W_T/L_A to L_A

Table 3 Value of constant

Constant	A_{1j}	t_{1j}	A_{2j}	t_{2j}	y_{0j}
$j=5$	1.020 29	2.947 07	41.826 48	8.479 63	6.275 2
$j=6$	0.012 5	6.444 25	17.090 11	5.401 42	3.229 94

(3) Under certain conditions, the relationships of S/L_A-L_A, L_H/L_A-L_A, W_H/L_A-L_A, L_T/L_A-L_A, and W_T/L_A-L_A are given.

References:

[1] Mori K, Osakada K. Simulation of Three-Dimensional Rolling by the Rigid-Plastic Finite Element Method [A]. Pittman J F T, Wood R D, Alexander J M, et al, eds. Proceedings of the International Conference on Numerical Methods in Industrial Forming Processes [C]. Swabsea: Pineridge, 1982. 747-756.

[2] David C, Bertrand C, Chenot J L, et al. A Transient 3D FEM Analysis of Hot Rolling of Thick Slabs [A]. Proceedings of Numiform'86 [C]. Rotterdam, Netherland: Balkema A A, 1986. 219-224.

[3] XIONG Shang-wu, LIU Xiang-hua, WANG Guo-dong, et al. Analysis of the Non-Steady State Vertical-Horizontal Rolling Process in Roughing Trains by the Three-Dimensional Finite Element Method [J]. Journal of Materials Processing Technology, 2002, 120(1-3): 53-61.

[4] YU Hai-liang, LIU Xiang-hua, LI Chang-sheng. FEM Analysis to the Slab Corner Metal Flow Condition During Multi-Pass V-H Rolling Process [J]. Journal of Northeastern University (Natural Science), 2005, 26(10): 982-985 (in Chinese).

[5] LIU Hui, GAO Cai-ru, WANG Guo-dong, et al. Effection of Edger Share on the Slab Profile [J]. Journal of Plasticity Engineering, 2003, 10(5): 86-88 (in Chinese).

[6] FENG Xian-zhang, LIU Cai. Finite Element Analysis of Slab Bulge Distribution During Sizing Press [J]. Metallurgical Equipment, 2004, 12(4): 1-3, 72 (in Chinese).

[7] XIONG Shang-wu, LU Cheng, LIU Xiang-hua, et al. Analysis of Horizontal Rolling for Slabs With Dog-Bone Shape by 3D Rigid-Plastic FEM [J]. Journal of Iron and Steel Research, 2000, 12(1): 14-17 (in Chinese).

(Continued From Page 5)

[2] YUAN Zhang-fu, GU Ke-jing. Characteristics of Swirl-Flow Oxygen Lance and Analysis of Its Application in Slag Splashing Technology [J]. Iron and Steel, 1998, 33(12): 17-20, 24 (in Chinese).

[3] Sakai A, Tani J, Yamada K, et al. Development of Low-Spitting Lance at Kashima's No. 2 Steelmaking Plant [A]. 77th Steelmaking Conference [C]. Warrendale, PA, USA: ISS, 1994. 61-66.

[4] Choi H S, Ryu J Y, Kim M R, et al. Modification of Lance Nozzle to Increase Productivity and BOF Lining Life at No. 2 Steelmaking Plant in Pohang Works [A]. 77th Steelmaking Conference [C]. Warrendale, PA, USA: ISS, 1994. 93-94.

[5] Higuchi Y, Tago Y. Effect of Nozzle Twisted Lance on Jet Behavior and Spitting Rate in Top Blown Process [J]. ISIJ Int, 2003, 43(9): 1410-1414.

[6] Swift T. BOF Oxygen Lance Improvements at Sparrows Point [A]. 84th Steelmaking Conference [C]. Warrendale, PA, USA: ISS, 2001. 525-540.

[7] Keilman L M, Galloway S M, Balajee S R, et al. Oxygen Lance Design Modifications to Improve the Lance Life and Performance at Inlands No. 2 BOF/CC Shop [A]. 76th Steelmaking Conference [C]. Warrendale, PA, USA: ISS, 1993. 145-161.